S. Saitta, F. Fabbrocino, R. Vescovini, N. Fantuzzi, R. Luciano
Radial Point Interpolation Method for Isotropic Nanoplates in Bending Using Strain Gradient Theory
International Journal of Computational Methods, Vol. 19, N. 10, 2022, 2250023 (22 pages)
doi:10.1142/S0219876222500232

Radial Point Interpolation Method for isotropic nanoplates in bending using strain gradient theory

SERENA SAITTA

Department of Engineering, Telematic University Pegaso
Naples, Italy
saittaseren@gmail.com

FRANCESCO FABBROCINO

Department of Engineering, Telematic University Pegaso
Naples, Italy
francesco.fabbrocino@unipegaso.it

RICCARDO VESCOVINI

Department of Aerospace Science and Technologies, Politecnico di Milano
Milan, Italy
riccardo.vescovini@polimi.it

NICHOLAS FANTUZZI*

Department of Civil, Chemical, Environmental and Materials Engineering, University of Bologna
Bologna, Italy
nicholas.fantuzzi@unibo.it
http://www.unibo.it/sitoweb/nicholas.fantuzzi/en

RAIMONDO LUCIANO

Engineering Department, Parthenope University
Naples, Italy
raimondo.luciano@uniparthenope.it

Received Day Month Year
Revised Day Month Year

This paper presents the static bending of isotropic Kirchhoff's nanoplates modelled using the second order strain gradient theory. The numerical analysis is conducted using Mesh Free methods instead of traditional Finite Elements. To the best of the authors' knowledge, no such meshless methods have been employed in the analysis of strain gradient nanoplates. Hermite Radial point interpolation method is used to approximate the bending degrees of freedom. Plates with different geometries and simply supported

*Corresponding Author

boundary conditions are studied. The results are then compared with the analytical solution available in the literature.

Keywords: Radial Point Interpolation Method; Meshless method; Strain Gradient theory; Nanoplates

1. Introduction

Recently, the focus of research on the topic of numerical methods is shifting from the traditional, well known FEM to alternative methods which can overcome its limitations while granting the same accuracy. In this context, the interest in Mesh Less or Mesh Free methods is rapidly growing. Application of these methods on the classical structural mechanical analysis has been widely studied [1, 2, 3]. The idea of the methods is to get rid of the classical mesh used in FEM by substituting it with a random nodal distribution used to represent the domain. It is true, however, that unless the problem is studied in its strong formulation, a mesh is still needed to evaluate the necessary integrals. But even in this case, the mesh and the nodal distribution are two distinct objects.

Different kind of shape functions have been developed and applied to solve some of the most famous structural mechanics problems [4, 5, 6]. Among them, the Point Interpolation Method (PIM) has the advantage of possessing the Kronecker delta function property, allowing for an easy imposition of the essential boundary conditions [7, 8, 9, 10]. Although very effective, simple and accurate, the PIM showes issues for regular nodal distributions. However, the method has been augmented with an additional sub-routine to effectively solve the problem [2, 11].

Another powerful Mesh Free Method is the Radial Point Interpolation Method (RPIM) which belongs to the same family as the PIM. It still possesses the Kronecker delta function property but overcomes the issues of the PIM [12, 13, 14, 15]. Which means that simple regularly distributed nodes can be used to represent the domain.

In a different field but a similar fashion, increasing studies in micro and nano structural components shifted researchers' focus from classical linear elasticity to nonlocal theories. These kind of structures, in fact, have proven to be extremely versatile, finding wide applications in MEMS (Micro-Electro-Mechanical-Systems) and NEMS (Nano-Electro-Mechanical-Systems) which require the employment of nanorods, nanobeams and nanoplates [16, 17, 18, 19, 20, 21, 22, 23]. Nonlocal theories have been widely applied in the study of these structural components to investigate nonlocal effects in both static [24, 25, 26, 27, 28] and dynamic [29, 30, 31, 32, 33, 34] analysis.

The mechanical behaviour of micro and nano components is affected by the microstructure of the material and by the interaction forces among particles which are far from each other [35, 36, 37, 38, 39]. All these effects are negligible on a macroscale but became significant in micro and nano structures.

The issue with classical theories is that they are not able to properly model

the microscopic effects dominating in these materials and that is because they do not involve any length scale parameter. On the other hand, nonlocal theories are characterised by the introduction of this extra degree of freedom or parameter [40, 20, 41, 42, 43]. Among all of these theories, the second order strain gradient theories are particularly easy to formulate, being characterised by the introduction of just one nonlocal parameter which directly enters in the constitutive law. The second order strain gradient theories have been widely applied to thin plates for which the analytical solution is available for certain combinations of boundary conditions [44, 45, 46, 47]. Numerical Finite Element Method (FEM) analysis has also been widely used in such applications [48, 49, 50, 51].

To the best of the authors' knowledge, Mesh Free Methods and nonlocal theories have not yet been used together to solve structural mechanics problems. The challenge of the present work is to implement a RPIM to solve the static bending problem of a nanoplate modelled via negative strain gradient theory.

This paper is organized as follows. The present introduction section is followed by the theoretical notions regarding thin isotropic Kirchhoff plates [52, 53]. The latter is followed by a detailed explanation of the Radial Point Interpolation Method, shape functions construction and numerical implementation. Section 3 presents the numerical results and graphs that validate and compare the present analysis against the available analytical solutions. Finally, a conclusion sections closes this work.

2. Formulation

2.1. *Kirchhoff plates theory*

A thin rectangular isotropic plate subjected to a uniformly distributed load q_z is considered. The dimensions of the plate are taken as a along the x-axis, b along the y-axis and h for the thickness which is considered uniform along the whole plate. According to Kirchhoff's flexural plate theory [54], the displacements along the x, y and z directions are the once usually considered for isotropic plates in bending configuration (in-plane plate motion is neglected). Thus, the unique plate degree of freedom is the transverse displacement w of the mid-plane (x,y,0). The strain-displacement relations can be written as:

$$\boldsymbol{\varepsilon} = z\mathbb{D}w(x,y) \tag{1}$$

where $\boldsymbol{\varepsilon} = [\varepsilon_{xx}\ \varepsilon_{yy}\ \gamma_{xy}]^\top$ and the differential operator:

$$\mathbb{D} = -\left[\frac{\partial^2}{\partial x^2}\ \frac{\partial^2}{\partial y^2}\ 2\frac{\partial^2}{\partial x \partial y}\right]^\top \tag{2}$$

has been introduced.

2.2. *Second order strain gradient theory*

The nanoplate mechanics is modelled according to the second-order strain gradient theory in which the non locality effects are expressed by the constitutive equation:

$$\boldsymbol{\sigma} = (1 - \ell^2 \Delta^2)\mathbf{Q}\boldsymbol{\varepsilon} \tag{3}$$

where $\boldsymbol{\sigma} = \left\{\sigma_{xx}\ \sigma_{yy}\ \tau_{xy}\right\}^\top$, ℓ is the nonlocal parameter, $\Delta^2 = \partial^2/\partial y^2 + \partial^2/\partial x^2$ denotes the Laplacian operator and $\mathbf{Q}$ is the classical matrix of reduced elastic constants.

The equations of motions are obtained by means of the principle of virtual work:

$$\delta U + \delta V = 0 \tag{4}$$

where δU is the virtual strain energy and δV is the virtual work of the external forces.

Being the only one affected by the strain gradient theory, let us focus on the first term of Equation (4). The strain energy of the plate in bending can be obtained as:

$$U = \int_A \boldsymbol{\varepsilon}^\top \boldsymbol{\sigma} dA \tag{5}$$

where A stands for the area of the plate. Considering the definition of strains and stresses given in Equations (2) and (3) respectively, the explicit form of the strain energy is given by:

$$\begin{aligned} U = \int_A \Bigg[& D_{11}\left(\frac{\partial^2 w}{\partial x^2}\right)^2 + 2D_{12}\frac{\partial^2 w}{\partial x^2}\frac{\partial^2 w}{\partial y^2} + D_{22}\left(\frac{\partial^2 w}{\partial y^2}\right)^2 + 4D_{66}\left(\frac{\partial^2 w}{\partial xy}\right)^2 \\ & + \ell^2 \Bigg(D_{11}\left(\frac{\partial^4 w}{\partial x^4} + \frac{\partial^4 w}{\partial x^2 \partial y^2}\right)\frac{\partial^2 w}{\partial x^2} + D_{12}\Bigg(\left(\frac{\partial^4 w}{\partial y^2 \partial x^2} + \frac{\partial^4 w}{\partial y^4}\right)\frac{\partial^2 w}{\partial x^2} + \\ & \left(\frac{\partial^4 w}{\partial x^4} + \frac{\partial^4 w}{\partial x^2 \partial y^2}\right)\frac{\partial^2 w}{\partial y^2}\Bigg) + D_{22}\left(\frac{\partial^4 w}{\partial x^2 \partial y^2} + \frac{\partial^4 w}{\partial y^4}\right) + \\ & 2D_{66}\left(\frac{\partial^4 w}{\partial x^3 \partial y} + 2\frac{\partial^4 w}{\partial x \partial y^3}\right)\frac{\partial^2 w}{\partial x \partial y}\Bigg)\Bigg] dA \end{aligned} \tag{6}$$

where D_{ij} are the components of the bending rigidity matrix $\mathbf{D}$, which, for plane stress problems, is expressed as:

$$\mathbf{D} = \frac{Eh^3}{12(1-\nu^2)}\begin{bmatrix} 1 & \nu & 0 \\ \nu & 1 & 0 \\ 0 & 0 & \frac{1-\nu}{2} \end{bmatrix} \tag{7}$$

where E is the Young's modulus and ν is the Poisson's ratio.

The variational form of the equation of motion can then be written as:

$$\int_A \Big\{ (\mathbb{D}\delta w(x,y))^\top \mathbf{D}\mathbb{D}w(x,y) + \ell^2 \Big[(\mathbb{D}_{,x}\delta w(x,y))^\top \mathbf{D}\mathbb{D}_{,x}w(x,y) + (\mathbb{D}_{,y}\delta w(x,y))^\top \mathbf{D}\mathbb{D}_{,y}w(x,y) \Big] + \delta w(x,y) q_z \Big\} dA = 0 \tag{8}$$

where

$$\mathbb{D}_{,x} = \frac{\partial}{\partial x}\mathbb{D} \qquad \mathbb{D}_{,y} = \frac{\partial}{\partial y}\mathbb{D} \tag{9}$$

Note that the first term in Equation (8) represents the classical strain energy component while the second includes the terms associated with the strain gradient theory.

2.3. *Mesh free formulation*

The analysis is performed using mesh free method, namely the Radial Point Interpolation Method (RPIM). The advantage of using such method is that no mesh is needed to perform the analysis. The domain is represented, not discretised, by an arbitrarily distributed set of nodes. A further simplification comes from the use of the RPIM, which possesses the Kronecker delta function property hence allowing for an easy imposition of the essential boundary conditions.

In the case of a Kirchhoff plate the only degree of freedom is the transverse deflection w. According to this theory, to properly impose the plate boundary constraints, its derivatives have to be considered as additional degrees of freedom, since such are primary variables of the problem. In addition, since a strain gradient theory is considered in the present work, not only first order derivatives of w (the rotations) are involved in the formulation but also the second order derivatives (the curvatures). In traditional finite element procedures in such cases Hermite interpolation functions should be employed in order to incorporate the derivatives in the finite element approximation. On the contrary in collocation methods, the shape functions do not directly embed all the needed degrees of freedom at the node. Therefore in this work the approximation involves the transverse motion w and its two first derivatives with respect to x and y.

In the context of the strain gradient theory, the essential boundary conditions for the plate are shown in Table 1 where the four edges are identified by the values of the physical coordinates x and y.

In this work, the degrees of freedom for the problem are taken as the deflection w and its first derivatives w_x and w_y. Any other higher-order derivative can be simply obtained by derivation. The essential boundary conditions will be imposed accordingly. Since both the deflection and its first derivatives are considered unknown, the Hermite-RPIM formulation is here presented.

BCs	$x = 0, a$	$y = 0, b$
Supported	$w = \frac{\partial w}{\partial y} = 0$	$w = \frac{\partial w}{\partial x} = 0$
Clamped	$w = \frac{\partial w}{\partial x} = \frac{\partial w}{\partial y} = 0$	$w = \frac{\partial w}{\partial x} = \frac{\partial w}{\partial y} = 0$
Free	No variables involved	No variables involved

Table 1: Essential boundary conditions considered.

Let's consider a domain enclosing n arbitrarily scattered nodes. The approximation of the deflection $w(x, y)$ can be expressed as:

$$\begin{aligned} w(x,y) &= \sum_{i=1}^{n} R_i(x,y)a_i + \sum_{i=1}^{n} R_{i,x}(x,y)a_i^x + \sum_{i=1}^{n} R_{i,y}(x,y)a_i^y \\ &= \mathbf{R}^\top(\mathbf{x})\mathbf{a} + \mathbf{R}_{,x}^\top(\mathbf{x})\mathbf{a}^x + \mathbf{R}_{,y}^\top(\mathbf{x})\mathbf{a}^y \end{aligned} \tag{10}$$

where $R_i(x, y)$, $R_{i,x}(x, y)$ and $R_{i,y}(x, y)$ are the radial basis function (RBF) and its derivatives and a_i, a_i^x and a_i^y the corresponding unknown vectors of coefficients. In this work, the multi-quadrics RBF is used in its general form:

$$R_i(x) = [(x - x_i)^2 + (y - y_i)^2 + (\alpha_c d_c)^2]^q \tag{11}$$

where q and α_c are two shape parameters, which have to be tuned, and d_c is a characteristic length given by the average distance between the nodes. For equally distributed nodes, it is just the distance between two consecutive nodes. The group of parameters $\alpha_c d_c$ is in this work indicated by a single letter C.

The derivatives of the function $w(x, y)$ are considered to be equal to the derivative of its approximation function. The vectors of coefficients in Equation (10) can be obtained by enforcing the field function and its derivatives to be satisfied at all the n nodes falling within the support domain of the point of interest $\mathbf{x}$. The support domain is a local domain, typically circular or rectangular, centered in a point of interest which can either be a node or an integration point. This leads to $3n$ linear equations which in matrix form are written as:

$$\mathbf{W} = \begin{Bmatrix} \mathbf{w} \\ \mathbf{w}_{,x} \\ \mathbf{w}_{,y} \end{Bmatrix} = \begin{bmatrix} \mathbf{R} & \mathbf{R}_{,x} & \mathbf{R}_{,y} \\ \mathbf{R}_{,x} & \mathbf{R}_{,xx} & \mathbf{R}_{,xy} \\ \mathbf{R}_{,y} & \mathbf{R}_{,xy} & \mathbf{R}_{,yy} \end{bmatrix} \begin{Bmatrix} \mathbf{a} \\ \mathbf{a}^x \\ \mathbf{a}^y \end{Bmatrix} = \mathbf{G} \begin{Bmatrix} \mathbf{a} \\ \mathbf{a}^x \\ \mathbf{a}^y \end{Bmatrix} \tag{12}$$

where $\mathbf{w}$, $\mathbf{w}_{,x}$ and $\mathbf{w}_{,y}$ are vectors of function values in the form:

$$\mathbf{w} = \begin{Bmatrix} w_1 & w_2 & \dots & w_n \end{Bmatrix}^\top \tag{13}$$

$$\mathbf{w}_{,x} = \begin{Bmatrix} w_{1,x} & w_{2,x} & \dots & w_{n,x} \end{Bmatrix}^\top \tag{14}$$

$$\mathbf{w}_{,y} = \begin{Bmatrix} w_{1,y} & w_{2,y} & \dots & w_{n,y} \end{Bmatrix}^\top \tag{15}$$

Solving Equation (12) and substituting into Equation (10):

$$\begin{aligned} w(x,y) &= \left\{\mathbf{R}^\top \ \mathbf{R}_{,x}^\top \ \mathbf{R}_{,y}^\top\right\} \begin{Bmatrix} \mathbf{a} \\ \mathbf{a}^x \\ \mathbf{a}^y \end{Bmatrix} \\ &= \left\{\mathbf{R}^\top \ \mathbf{R}_{,x}^\top \ \mathbf{R}_{,y}^\top\right\} \mathbf{G}^{-1}\mathbf{W} \end{aligned} \tag{16}$$

It follows that the Hermite-RPIM shape functions are written as:

$$\begin{aligned} \mathbf{\Phi}^\top(\mathbf{x}) &= \left\{\mathbf{R}^\top \ \mathbf{R}_{,x}^\top \ \mathbf{R}_{,y}^\top\right\} \mathbf{G}^{-1} = \left\{\boldsymbol{\varphi} \ \boldsymbol{\varphi}^x \ \boldsymbol{\varphi}^y\right\} \\ &= \left\{\varphi_1 \dots \varphi_i \dots \varphi_n \ \varphi_1^x \dots \varphi_i^x \dots \varphi_n^x \ \varphi_1^y \dots \varphi_i^y \dots \varphi_n^y\right\} \end{aligned} \tag{17}$$

An example of what the shape functions look like as computed with this method is given in Figure 1. Here, a squared domain of size $L = 1$ is represented by means of 9 regularly distributed nodes: one node on each corner, one node in the middle of each side and one node in the middle. All of the nodes are used to construct the shape functions for this domain. Figure 1 represents the shape functions and their first derivatives with respect to x and y for the nodes in the bottom left corner, in the middle left side, in the middle of the domain and in the top right corner respectively. For this particular case, the dimensionless parameters of the RBF are chosen as $C = 1$ and $q = 0.05$.

In the same way as in conventional FEM[49], once the shape functions are carried out, they are introduced in the weak form of the equations of motion as it is written reported in Equation (8).

$$\begin{aligned} \delta\mathbf{W} \int_A \Big\{ \Big[&(\mathbb{D}\mathbf{\Phi}^\top)^\top \mathbf{D} (\mathbb{D}\mathbf{\Phi}^\top) \\ &+ \ell^2 ((\mathbb{D}_{,x}\mathbf{\Phi}^\top)^\top \mathbf{D} (\mathbb{D}_{,x}\mathbf{\Phi}) + (\mathbb{D}_{,y}\mathbf{\Phi}^\top)^\top \mathbf{D} (\mathbb{D}_{,y}\mathbf{\Phi})) \Big] \mathbf{W} + \mathbf{\Phi} q_z \Big\} dA = 0 \end{aligned} \tag{18}$$

Although mesh free methods do not need any mesh for the representation of the problem domain, a so-called background mesh is still needed to perform the integration. This mesh and the nodal distribution that represents the problem domain are two independent sets.

The variational principle written in discrete form (Equation (18)) leads to the following algebraic set of equations:

$$[\mathbf{K_c} + \mathbf{K_{sg}}]\mathbf{W} = \mathbf{F} \tag{19}$$

where the classical and strain gradient related components of the stiffness matrix for node i are given by:

$$\mathbf{K}_{\mathbf{c}i} = \int_A \mathbb{B}_i^\top \mathbf{D} \mathbb{B}_i dA \tag{20}$$

$$\mathbf{K}_{\mathbf{sg}_i} = \int_A \ell^2 \left(\mathbb{B}_{,x_i}^\top \mathbf{D} \mathbb{B}_{,x_i} + \mathbb{B}_{,y_i}^\top \mathbf{D} \mathbb{B}_{,y_i} \right) dA \tag{21}$$

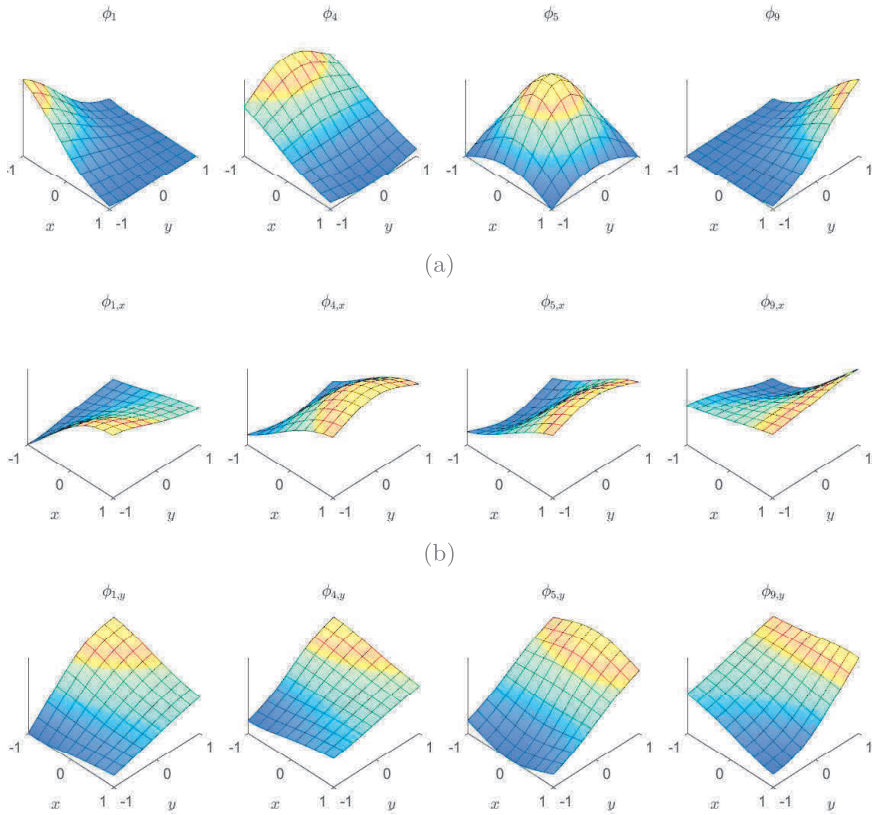

Fig. 1: (a) Shape functions. (b) Shape functions derivative with respect to x. (c) Shape functions derivative with respect to y.

where

$$\mathbb{B}_i = \mathbb{D}\mathbf{\Phi}_i^\top \qquad \mathbb{B}_{,x\,i} = \mathbb{D}_{,x}\mathbf{\Phi}_i^\top \qquad \mathbb{B}_{,y\,i} = \mathbb{D}_{,y}\mathbf{\Phi}_i^\top \tag{22}$$

In a similar way, the load vector is given by:

$$\mathbf{F} = \int_A \mathbf{\Phi}_i q_z dA \tag{23}$$

2.3.1. *Background Mesh and Integration*

As mentioned in Section 2.3, the integrals appearing in the weak form of the equation of motion have to be evaluated numerically. In this work, a 3×3 Gauss integration scheme is used to perform the integration. This leads to the necessity of introducing a mesh, called background mesh, whose purpose is to allow for the calculation of the needed Gauss points and weights. Although, the background mesh

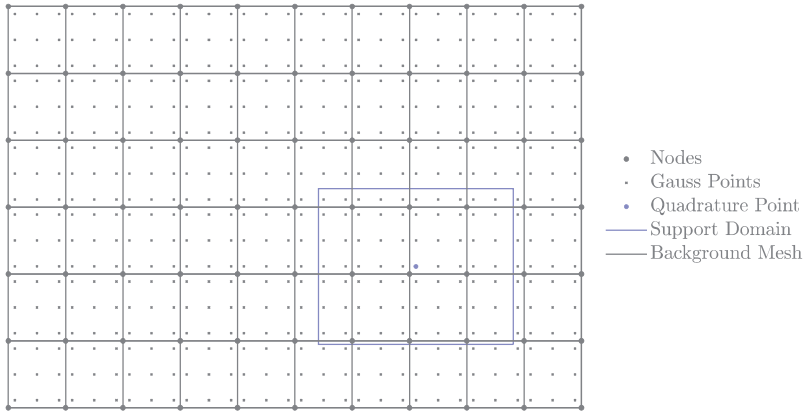

Fig. 2: Example of nodal distribution, background mesh, Gauss points and support domain for a generic rectangular plate.

and the nodal distribution representing the domain are two independent objects, in this work the points of the mesh and the nodes in the domain are considered to be in the same locations, as shown in Figure 2.

It can be noticed that the background mesh is made of 4-node elements. Moreover, being the nodal distribution regular in the domain, the elements are all rectangular elements.

The position of the integration points x_{G_i} in the element local domain and the corresponding weights p_{G_i} are reported in Equation (24) and (25) respectively:

$$x_{G_i} = \{-\sqrt{3/5} \quad 0 \quad \sqrt{3/5}\} \tag{24}$$

$$p_{G_i} = \{5/9 \quad 8/9 \quad 5/9\} \tag{25}$$

As in conventional FEM, an isoparametric transformation is used to move from the local domain of the element to the global domain of the problem.

Figure 2 also illustrates an example of support domain. It shows how in Mesh Free formulation the Gauss points have a twofold function. On the one hand, they are used to evaluate the stiffness matrix and load vector integrals. On the other, they are used as centering points for the support domain. In this case, they are also called quadrature points.

The support domain is of capital importance in the construction of the shape functions. In fact, at each step of the algorithm, only the nodes falling inside the local domain are used for the construction of the shape function. The denomination of *moving* local domain, which is often used when referring to the support domain, is due to this peculiarity. At each step, the moving domain is centered in a different Gauss (or quadrature) point. It "jumps" from point to point, each time enclosing different nodes.

Note that although it is common practice for the local domain to be centered in the Gauss points, it is not mandatory. In fact, the nodes themselves are also used for this purpose.

3. Numerical Results

3.1. *Simply Supported nanoplates*

This section aims to show the results of the numerical analysis of a simply-supported (SSSS) isotropic Kirchhoff nanoplate modelled according to the second-order strain gradient theory and analysed by means of a mesh free RPIM. The numerical codes are developed in MATLAB.

The results in terms of maximum transverse displacement are presented in the nondimensional form as follows:

$$\bar{w} = \frac{1000wD}{q_z a^4} \tag{26}$$

where w is the maximum (central) plate deflection, q_z is the magnitude of the external load and D is the bending rigidity $D = Eh^3/12(1-\nu^2)$.

Nanoplates with different geometries are analysed, all having thickness $h = 0.34$ nm. Young's modulus and Poisson's ratio are taken as 1100 GPa and 0.3 respectively. Different nodal densities are also taken into account. Nanoplates represented by 5×5, 9×9, 11×11 and 15×15 equally spaced node grids are studied to analyse the convergence of the method. The local parameter ℓ also varies according to the analysis and results presented in the available literature [44].

The support domain used for the mesh free implementation has rectangular shape and is centered in the Gauss points. Its dimensions are considered in the classical way [2] $d_s = \alpha_s d_c$ where d_c is the average nodal spacing $d_c = \sqrt{\Delta x^2 + \Delta y^2}$ and α_s is a dimensionless parameter which, in this work, varies from 1.8 to 2.4. Note that, in this work, 3×3 Gauss integration points are used in each cell of the background integration mesh.

Results listed in Tables 2-5 compare the available analytical solutions [44] with the present ones in terms of percentage error:

$$err_{\%} = 100\frac{|w_e - \bar{w}|}{w_e} \tag{27}$$

where w_e is the exact solution taken from the aforementioned references.

The provided comparison is performed for different plate aspect ratios, number of collocation nodes and nonlocal parameter values. The C and q coefficients characterising the MQ radial basis functions vary as the ratio b/a changes.

It should be remarked that although in the case of $\ell^2 = 0$ the results converge monotonically, this is not always true for different values of the local parameter. This behaviour might be justified by the relative influence that the nodal coordinates and the number of nodes have on the result.

For a fixed geometry, it is obvious that locating a small or a large number of nodes accuracy changes. In mesh free methods, this numerical trend is due to the fact that nodal spacing appears in the derivative calculation. Since the strain gradient theory requires the computation of high order derivatives of the RBF, the spacial coordinates of the nodes appear to be multiplied several times (once per each derivative order). The larger these are the larger the number appearing in the shape functions will be. But as the nodal density increases, the coordinates of the nodes will get smaller as well as the values in the shape functions, yielding larger errors. It is clear as these two effects counteract each other in the cases in which $\ell^2 \neq 0$. Hence, the convergence may not be monotonic due to the balancing of these two behaviours.

Overall, as the number of nodes increases, the results show good convergence with the analytical solution. As expected, the percentage error increases as the local parameter increases and, even for high number of nodes, the value of the error when $\ell^2 = 1$ remains quite high.

Table 2: Non dimensional values of $\bar{w}$ for SSSS nanoplate with $b/a = 0.5$ obtained for $C = 2$, $q = -0.9$

Nodes	Nonlocal parameter ℓ (nm)	Result	Error (%)
5×5	0	0.5921	6.4613
	0.2	0.5601	9.9228
	0.5	0.4461	21.4613
	1	0.2655	38.4847
9×9	0	0.6291	0.6161
	0.2	0.6161	0.9167
	0.5	0.5641	0.6866
	1	0.4484	3.8925
11×11	0	0.6325	0.0790
	0.2	0.6212	0.0965
	0.5	0.5758	1.3732
	1	0.4741	9.8471
15×15	0	0.6331	0.0158
	0.2	0.6189	0.4664
	0.5	0.5721	0.7218
	1	0.4669	8.1789
Analytical	0	0.6330	–
	0.2	0.6218	–
	0.5	0.5680	–
	1	0.4316	–

The graphical output of the aforementioned tables is given in Figure 3 where the same error in logarithmic form is provided.

From such figure it is clear that a convergence trend can be observed for different geometries and by increasing the number of grid points. Results are quite accurate for local plates and errors tend to increase by increasing the nonlocality for the

Table 3: Non dimensional values of $\bar{w}$ for SSSS nanoplate with $b/a = 1$ obtained for $C = 2.5$, $q = -0.9$.

Nodes	Nonlocal parameter ℓ (nm)	Result	Error (%)
5×5	0	2.8622	3.2198
	0.2	3.9638	1.7158
	0.5	3.3264	14.3652
	1	2.4501	28.4245
9×9	0	4.0166	1.1274
	0.2	3.9550	1.9340
	0.5	3.6656	5.6328
	1	2.9224	14.6271
11×11	0	4.0543	0.1994
	0.2	3.9818	1.2695
	0.5	3.7327	3.9054
	1	3.0560	10.7242
15×15	0	4.0624	0.0000
	0.2	4.0323	0.0174
	0.5	3.8906	0.1596
	1	3.4699	1.3672
Analytical	0	4.0624	–
	0.2	4.0330	–
	0.5	3.8844	–
	1	3.4231	–

reasons mentioned above.

3.2. *Clamped nanoplates*

This section show the results of the analysis of clamped (CCCC) nanoplates obtained following the same procedure as in the previous section.

The results are still considered in terms of nondimensional maximum transverse displacement as shown in Equation (26). Again, the comparison is made in terms of percentage error as given in Equation (27). The plate properties, aspect ratio, nodal distribution and Gauss integration are the same as in the SSSS case.

As for the case of SSSS nanoplates analysis, a graphical output of the results listed in the tables is provided in Figure 4.

The same considerations done for the SSSS nanoplates hold for the CCCC case as well. The influence of the high-order derivatives can once again be observed in the trend of the converge which can be not always strictly monotonic.

The numerical errors remain contained and, as expected, the highest values are almost always observed in the case $\ell^2 = 1$.

3.3. *Random nodal distribution and FEM comparison*

The analyses performed in the previous sections are now performed again on a square plate which is represented by a set of randomly distributed nodes. An ini-

Table 4: Non dimensional values of $\bar{w}$ for SSSS nanoplate with $b/a = 2$ obtained for $C = 2$, $q = 1.03$.

Nodes	Nonlocal parameter ℓ (nm)	Result	Error (%)
5×5	0	9.4322	6.8765
	0.2	9.3656	7.1177
	0.5	9.0424	8.2008
	1	8.0692	11.2162
9×9	0	9.9510	1.7544
	0.2	9.9027	1.7911
	0.5	9.6721	1.8081
	1	8.9970	1.0079
11×11	0	10.0594	0.6842
	0.2	10.0128	0.6992
	0.5	9.7945	0.5655
	1	9.1645	0.8351
15×15	0	10.1214	0.0721
	0.2	10.0761	0.0714
	0.5	9.8672	0.1726
	1	9.2689	1.9838
Analytical	0	10.1287	–
	0.2	10.0833	–
	0.5	9.8502	–
	1	9.0886	–

tially regular nodal population of 15×15 nodes, is randomly perturbed by introducing a small perturbation of magnitude 0.3. The nodal distribution obtained is shown in Figure 5.

As an advantage provided by Mesh Free Methods, the mesh is kept regular and is detached from the nodal distribution. As for the previous analyses, a 3×3 Gauss integration rule is employed for numerical integrals evaluation. Both SSSS and CCCC boundary conditions are accounted for. The results are presented in their nondimentional form as expressed in Equation (26) and compared in terms of percentage error (27) with respect to a reference solution as given in literature [44]. The results of the analyses are shown in Table 10.

The trend of the error remains coherent with the previous analyses and convergence is ensured as well. Considering the results of Table 10, it can be seen how the nodal distribution pays little to no influence on the accuracy of the results, which remains high. On the other hand, the observations done in the previous section on the influence of the nonlocal parameter ℓ as well as that of the high order derivatives involved in the calculation, still stand.

As an additional investigation, the results obtained with both the regular and random nodal distributions are compared against a FEM reference solution, as shown in Tables 11 and 12.

It can be observed how all the different methods grants highly accurate results. The comparison allows to understand in a clearer way how the influence of the

Table 5: Non dimensional values of $\bar{w}$ for SSSS nanoplate with $b/a = 3$ obtained for $C = 3$, $q = -0.05$.

Nodes	Nonlocal parameter ℓ (nm)	Result	Error (%)
5×5	0	12.5044	2.2202
	0.2	12.2747	0.7451
	0.5	11.2121	6.0365
	1	8.6155	22.4155
9×9	0	11.9913	1.9745
	0.2	11.9147	2.2098
	0.5	11.5916	2.8562
	1	10.7047	3.6009
11×11	0	12.0919	1.1519
	0.2	12.0313	1.2522
	0.5	11.7796	1.2801
	1	11.1060	0.0125
15×15	0	12.2041	0.2344
	0.2	12.1536	0.2483
	0.5	11.9399	0.0627
	1	11.3603	2.3029
Analytical	0	12.2328	–
	0.2	12.1839	–
	0.5	11.9324	–
	1	11.1046	–

higher order derivatives seems to affect the RPIM slightly more than it does the FEM. However, the accuracy of the results is in no way compromised and the RPIM is proven to be a potential valid alternative to traditional FEM.

4. Conclusion

In this work, strain gradient nanoplates have been analyzed by means of the Radial Point Interpolation Method. Isotropic second order strain gradient Kirchhoff nanoplates with simply-supported and clamped boundary conditions are analyzed. The aim was to apply a RPIM formulation to thin plates modelled via strain gradient theory. According to the current state of the art, an implementation of RPIM with higher-order partial differential equations has never been presented in the literature. The paper provides a detailed explanation of the RPIM method theoretical and numerical implementation as well as theoretical notions in both explicit and matrix form. This work proves the validity of the RPIM for problems with higher order of derivatives involved. Numerical convergence with the analytical results achieved in recent literature was studied. The present results for simply supported and clamped plates that have been obtained by using some of the traditionally most used dimensionless parameters involved in the MQ radial basis functions employed in the RPIM. The analyses are performed employing both a regular and random nodal distribution for domain representation. In addition, a comparison with conforming and nonconforming FEM is provided. Further works will study how the

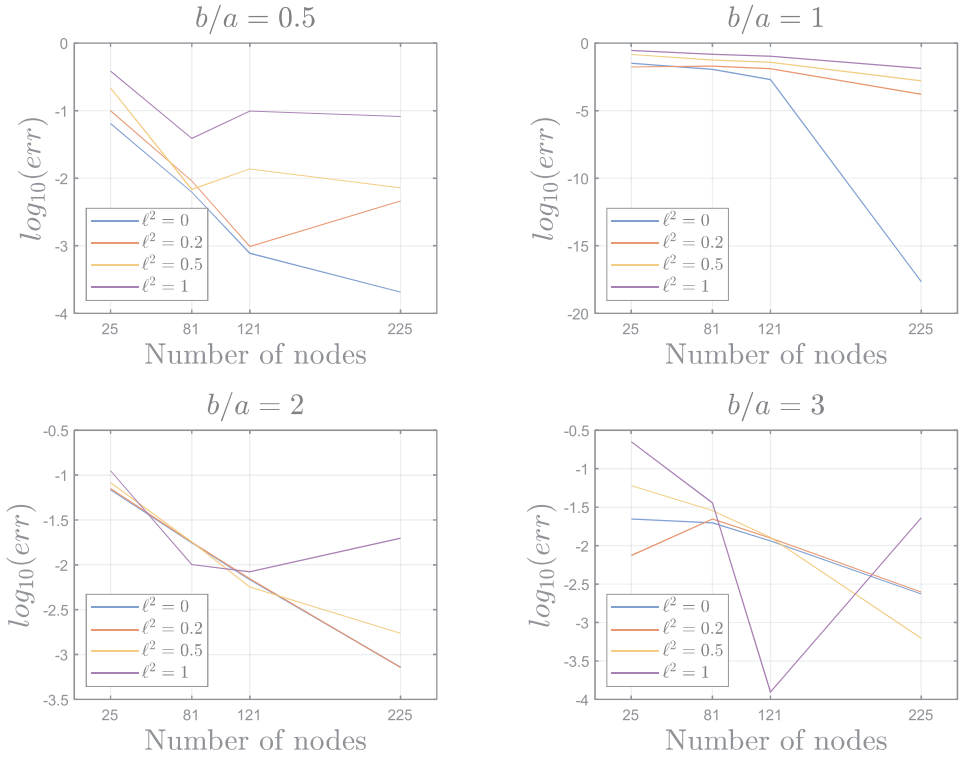

Fig. 3: Convergence analysis results of isotropic SSSS plates with different geometries and varying nodal distribution and local parameter value.

parameters influence the results when different kinds of constraints are involved, checking the effects the parameters have both in the convergence and accuracy of the results.

Table 6: Non dimensional values of $\bar{w}$ for CCCC nanoplate with $b/a = 0.5$ obtained for $C = 1$, $q = -0.05$

Nodes	Nonlocal parameter ℓ (nm)	Result	Error (%)
5×5	0	0.1891	19.4557
	0.2	0.1635	10.7286
	0.5	0.1025	7.5365
	1	0.0449	23.9665
9×9	0	0.1622	2.4380
	0.2	0.1486	0.6179
	0.5	0.1063	4.1618
	1	0.0533	9.6193
11×11	0	0.1603	1.2859
	0.2	0.1482	0.3688
	0.5	0.1088	1.9070
	1	0.0562	4.6760
15×15	0	0.1584	0.0893
	0.2	0.1472	0.3080
	0.5	0.1098	1.0071
	1	0.0579	1.8716
Analytical	0	0.1583	–
	0.2	0.1477	–
	0.5	0.1109	–
	1	0.0590	–

Table 7: Non dimensional values of $\bar{w}$ for CCCC nanoplate with $b/a = 1$ obtained for $C = 2.5$, $q = -0.9$

Nodes	Nonlocal parameter ℓ (nm)	Result	Error (%)
5×5	0	1.2178	3.7553
	0.2	1.1790	4.4045
	0.5	1.0323	5.9749
	1	0.7316	7.9286
9×9	0	1.2632	0.1698
	0.2	1.2263	0.5641
	0.5	1.0746	2.1186
	1	0.7548	5.0118
11×11	0	1.2698	0.3559
	0.2	1.2352	0.1550
	0.5	1.0920	0.5351
	1	0.7796	1.8888
15×15	0	1.2689	0.2863
	0.2	1.2366	0.2715
	0.5	1.1019	0.3602
	1	0.8015	0.8742
Analytical	0	1.2653	–
	0.2	1.2333	–
	0.5	1.0979	–
	1	0.7946	–

Table 8: Non dimensional values of $\bar{w}$ for CCCC nanoplate with $b/a = 2$ obtained for $C = 2$, $q = 1.03$

Nodes	Nonlocal parameter ℓ (nm)	Result	Error (%)
5×5	0	2.8283	11.6599
	0.2	2.7543	10.7863
	0.5	2.4541	7.6428
	1	1.8133	2.2072
9×9	0	2.5646	1.2472
	0.2	2.5144	1.1376
	0.5	2.2978	0.7871
	1	1.7773	0.1792
11×11	0	2.5517	0.7387
	0.2	2.5035	0.7011
	0.5	2.2959	0.7035
	1	1.7901	0.8996
15×15	0	2.5604	1.0807
	0.2	2.5012	0.6088
	0.5	2.2894	0.4185
	1	1.7784	0.2416
Analytical	0	2.5330	–
	0.2	2.4861	–
	0.5	2.2799	–
	1	1.7741	–

Table 9: Non dimensional values of $\bar{w}$ for CCCC nanoplate with $b/a = 3$ obtained for $C = 3$, $q = -0.05$

Nodes	Nonlocal parameter ℓ (nm)	Result	Error (%)
5×5	0	3.6127	38.0352
	0.2	3.4960	35.9997
	0.5	3.0299	28.1722
	1	2.1042	13.6300
9×9	0	2.7543	5.2388
	0.2	2.6939	4.7982
	0.5	2.4557	3.8836
	1	1.8966	2.4187
11×11	0	2.6769	2.2829
	0.2	2.6080	1.4560
	0.5	2.3844	0.8654
	1	1.8587	0.3743
15×15	0	2.6335	0.6227
	0.2	2.5861	0.6015
	0.5	2.3896	1.0880
	1	1.9017	2.6957
Analytical	0	2.6172	–
	0.2	2.5706	–
	0.5	2.3639	–
	1	1.8518	–

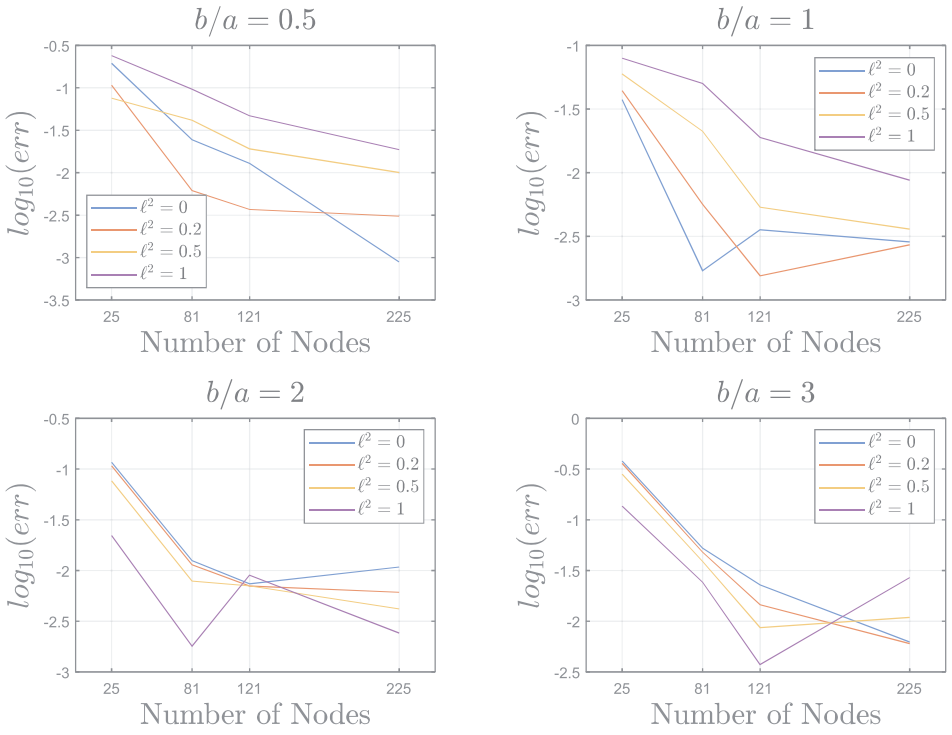

Fig. 4: Convergence analysis results of isotropic CCCC plates with different geometries and varying nodal distribution and local parameter value.

Table 10: Non dimensional values of $\bar{w}$ for SSSS and CCCC square nanoplate obtained for $C = 1.42$, $q = 0.9$.

Boundary Conditions	ℓ (nm)	Reference solution	Result	Error (%)
SSSS	0	4.0624	4.0627	0.0074
	0.2	4.0330	4.0213	0.2901
	0.5	3.8844	3.8756	0.2265
	1	3.4231	3.4549	0.9290
CCCC	0	1.2653	1.2723	0.5532
	0.2	1.2333	1.2310	0.1865
	0.5	1.0979	1.0930	0.4463
	1	0.7946	0.7906	0.5034

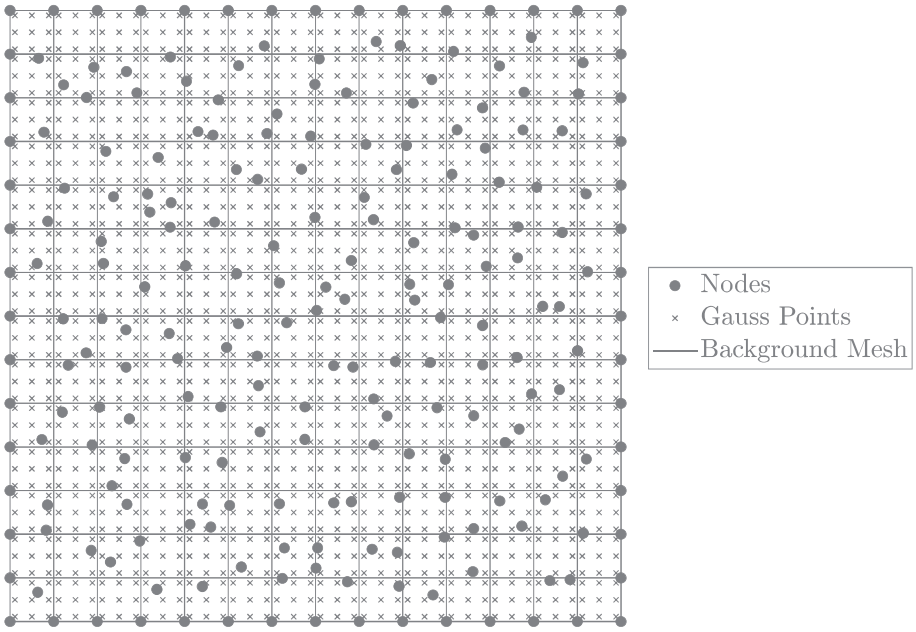

Fig. 5: Square Plate discretised by a random nodal distribution. A regular mesh is employed for integration.

Table 11: Comparison of non dimensional values of $\bar{w}$ for a squared SSSS nanoplate obtained with different numerical methods.

ℓ (nm)	Analytical	FEM Conforming [35]	FEM Nonconforming [35]	RPIM regular	RPIM random
0	4.0624	4.0624	4.0624	4.0624	4.0627
0.2	4.0330	4.0333	4.0331	4.0323	4.0213
0.5	3.8844	3.8865	3.8847	3.8906	3.8756
1	3.4231	3.4305	3.4240	3.4699	3.4549

Table 12: Comparison of non dimensional values of $\bar{w}$ for a squared CCCC nanoplate obtained with different numerical methods.

ℓ (nm)	Analytical	FEM Conforming [35]	FEM Nonconforming [35]	RPIM regular	RPIM random
0	1.2653	1.3725	1.2662	1.2689	1.2723
0.2	1.2333	1.2440	1.2335	1.2366	1.2310
0.5	1.0979	1.0999	1.0985	1.1019	1.0930
1	0.7946	0.7953	0.7959	0.8015	0.7906

References

[1] Bing-Bing Xu, Xiao-Wei Gao, Miao Cui. "High precision simulation of thermal-mechanical problems in functionally graded materials by spectral element differential method". In: *Computers and Structures* 239.106322 (2020).

[2] G. R. Liu. *Mesh Free Methods Moving beyond the Finite Element Method*. CRC Press LLC, 2003. ISBN: 0-8493-1238-8.

[3] Mart Ratas, Jüri Majak, and Andrus Salupere. "Solving Nonlinear Boundary Value Problems Using the Higher Order Haar Wavelet Method". In: *Mathematics* 9.21 (2021).

[4] G.R. Liu and Y.T. Gu. *An Introduction to Meshfree Methods and Their Programming*. Springer Netherlands, 2005. ISBN: 9781402034688.

[5] M. Sorrenti et al. "Static Response and Buckling Loads of Multilayered Composite Beams Using the Refined Zigzag Theory and Higher-Order Haar Wavelet Method". In: *Mechanics of Composite Materials* 57.1 (2021), pp. 1–18.

[6] M. Ratas, A. Salupere, and J. Majak. "Solving nonlinear PDEs using the higher order Haar wavelet method on nonuniform and adaptive grids". In: *Mathematical Modelling and Analysis* 26.1 (2021), pp. 147–169.

[7] Y. T. Gu, G. R. Liu. "A local point interpolation method for static and dynamic analysis of thin beams". In: *Comput. Methods Appl. Mech. Engrg.* 190 (2001), pp. 5515–5528. DOI: www.elsevier.com/locate/cma.

[8] G. R. Liu, Y. T. Gu. "A point interpolation method for two-dimensional solids". In: *Int. J. Numer. Meth. Engng.* 50 (2001), pp. 937–951.

[9] G. R. Liu, X. Xu, G. Y. Zhang, Y. T. Gu. "An extended Galerkin weak form and a point interpolation method with continuous strain field and superconvergence using triangular mesh". In: *Comput. Mech.* 43 (2009), pp. 651–673. DOI: 10.1007/s00466-008-0336-5.

[10] X. Xu, G. R. Liu, Y. T. Gu, G. Y. Zhang, J. W. Luo, J. X. Peng. "A point interpolation method with locally smoothed strain field (PIM-LS2) for mechanics problems using triangular mesh". In: *Finite Elements in Analysis and Design* 46 (2010), pp. 862–874. DOI: http://dx.doi.org/10.1016/j.finel.2010.05.005.

[11] G.R. Liu and Y.T. Gu. "A matrix triangularization algorithm for the polynomial point interpolation method". In: *Computer Methods in Applied Mechanics and Engineering* 192.19 (2003), pp. 2269–2295. ISSN: 0045-7825. DOI: https://doi.org/10.1016/S0045-7825(03)00266-4.

[12] Xiangyang Cui, Guirong Liu, Guangyao Li. "A smoothed Hermite radial point interpolation method for thin plate analysis". In: *Arch. Appl. Mech.* 81 (2011), pp. 1–18. DOI: 10.1007/s00419-009-0392-0.

[13] J. G. Wang, G. R. Liu. "A point interpolation meshless method based on radial basis functions". In: *Int. J. Numer. Meth. Engng.* 54 (2002), pp. 1623–1648. DOI: 10.1002/nme.489.

[14] G. R. Liu, G. Y. Zhang, Y. T. Gu, Y. Y. Wang. "A meshfree radial point interpolation method (RPIM) for three-dimensional solids". In: *Comput. Mech.* 36 (2005), pp. 421–430. DOI: 10.1007/s00466-005-0657-6.

[15] Yan Li, Guirong Liu, Zhiqiang Feng, Keishing Ng, Siuwai Li. "A node-based smoothed radial point interpolation method with linear strain fields for vibration analysis of solids". In: *Engineering Analysis with Boundary Elements* 114 (2020), pp. 8–22.

[16] P. M. Mariano, P. Trovalusci. "Constitutive Relations for Elastic Microcracked Bodies: From a Lattice Model to a Multifield Continuum Description". In: *Inter-*

national Journal of Damage Mechanics (). DOI: https://doi.org/10.1177\%2F1056789599008002004.

[17] R. Barretta, S. A.Fazelzadeh, L. Feo, E.Ghavanloo, R. Luciano. "Nonlocal inflected nano-beams: A stress-driven approach of bi-Helmholtz type". In: *Composite Structures* 200 (2018), pp. 239–244. DOI: https://doi.org/10.1016/j.compstruct.2018.04.072.

[18] A. Mahmure, A. H.Sofiyev, N.Fantuzzi, N. Kuruoglu. "Primary resonance of double-curved nanocomposite shells using nonlinear theory and multi-scales method: Modeling and analytical solution". In: *International Journal of Non-Linear Mechanics* 137.103816 (2021). DOI: https://doi.org/10.1016/j.ijnonlinmec.2021.103816.

[19] Cornacchia F., Liu T., Bai Y., Fantuzzi N. "Tensile strength of the unbonded flexible pipes". In: *COMPOSITE STRUCTURES* 218 (2019), pp. 142–151.

[20] Akgöz B., Civalek Ö. "Bending analysis of FG microbeams resting on Winkler elastic foundation via strain gradient elasticity". In: *Compos. Struct.* 134 (2015), pp. 249–301.

[21] Barretta R., Feo L., Luciano R., de Sciarra F. M. "A gradient Eringen model for functionally graded nanorods". In: *Compos. Struct.* 131 (2015), pp. 1124–31.

[22] Numanglu H. M., Akgoz B., Civalek Ö. "On dynamic analysis of nanorods". In: *Int. J. Eng. Sci.* 130 (2018), pp. 33–50.

[23] Apuzzo A., Barretta R., Luciano R., de Sciarra F. M., Penna R. "Free vibrations of Bernoulli-euler nano-beams by the stress-driven nonlocal integral model". In: *Compos. B Eng.* 123 (2017), pp. 105–111.

[24] P. Trovalusci, G. Augusti. "A continuum model with microstructure for materials with flaws and inclusions". In: *J. Phys. IV France* 08.PR8 (1998). DOI: https://doi.org/10.1051/jp4:1998847.

[25] M. Tuna, M. Kirca, P. Trovalusci. "Deformation of atomic models and their equivalent continuum counterparts using Eringen's two-phase local/nonlocal model". In: *Mechanics Research Communications* 97.PR8 (2019), pp. 26–32. DOI: https://doi.org/10.1016/j.mechrescom.2019.04.004.

[26] R. Barretta, R. Luciano, F. M. de Sciarra. "A Fully Gradient Model for Euler-Bernoulli Nanobeams". In: *Mathematical Problems in Engineering* (2015). DOI: https://doi.org/10.1155/2015/495095.

[27] G. Tocci Monaco, N. Fantuzzi, F. Fabbrocino, R. Luciano. "Trigonometric Solution for the Bending Analysis of Magneto-Electro-Elastic Strain Gradient Nonlocal Nanoplates in Hygro-Thermal Environment". In: *Special Issue Analytical and Numerical Methods for Linear and Nonlinear Analysis of Structures at Macro, Micro and Nano Scale* (). DOI: https://doi.org/10.3390/math9050567.

[28] Barretta R., Marotti de Sciarra F. "A nonlocal model for carbon nanotubes under axial loads". In: *Adv. Mater Sci. Eng.* (2013).

[29] M. Avey, N. Fantuzzi, A. H.Sofiyev, N. Kuruoglu. "Nonlinear vibration of multilayer shell-type structural elements with double curvature consisting of CNT patterned layers within different theories". In: *Composite Structures* 275.114401 (2021). DOI: https://doi.org/10.1016/j.compstruct.2021.114401.

[30] A. Deniz, N. Fantuzzi, A. H. Sofiyev, N. Kuruoglu. "Modeling and Solution of Large Amplitude Vibration Problem of Construction Elements Made of Nanocomposites Using Shear Deformation Theory". In: (). DOI: https://doi.org/10.3390/ma14143843.

[31] G. Tocci Monaco, N. Fantuzzi, F. Fabbrocino, R. Luciano. "Critical Temperatures for Vibrations and Buckling of Magneto-Electro-Elastic Nonlocal Strain Gradient Plates". In: (). DOI: https://doi.org/10.3390/nano11010087.

[32] Numanglu H. M., Akgoz B., Civalek Ö. "On dynamic analysis of nanorods". In: *Int. J. Eng.* 130 (2018), pp. 33–50.

[33] Barretta R., Faghidian S. A., Luciano R. "Longitudinal vibrations of nano-rods by stress-driven integral elasticity". In: *Mech. Adv. Mater. Struct.* 26 (2019), pp. 1307–15.

[34] Apuzzo A., Barretta R., Canadija M., Feo L., Luciano R., de Sciarra F. M. "A closed-form model for torsion of nanobeams with an enhanced nonlocal formulation". In: *Compos. B Eng.* 108 (2017), pp. 315–324.

[35] B. Babu, B. P. Patel. "A new computationally efficient finite element formulation for nanoplates using second-order strain gradient Kirchhoff's plate theory". In: *Composites Part B* 168 (2019), pp. 302–311.

[36] N. Fantuzzi, P. Trovalusci, S. Dharasura. "Mechanical Behavior of Anisotropic Composite Materials as Micropolar Continua". In: *Front. Mater.* (). DOI: https://doi.org/10.3389/fmats.2019.00059.

[37] G. Mancusi, F. Fabbrocino, L. Feo, F. Fraternalia. "Size effect and dynamic properties of 2D lattice materials". In: *Composites Part B: Engineering* 112 (2017), pp. 235–242. DOI: https://doi.org/10.1016/j.compositesb.2016.12.026.

[38] R. Luciano, J. R. Willis. "Non-local constitutive response of a random laminate subjected to configuration-dependent body force". In: *Journal of the Mechanics and Physics of Solids* 49.Issue 2 (2001), pp. 431–444. DOI: https://doi.org/10.1016/S0022-5096(00)00031-4.

[39] Akgöz B., Civalek Ö. "Analysis of micro-sized beams for various boundary conditions based on the strain gradient elasticity theory". In: *Arch. Appl. Mech.* 82 (2012), pp. 423–43.

[40] B. Akgöz and Ö. Civalek. "A microstructure-dependent sinusoidal plate model based on the strain gradient elasticity theory". In: *Acta Mech.* 226.7 (2015), pp. 2277–2294. DOI: 10.1007/s00707-015-1308-4.

[41] B. Akgöz and Ö. Civalek. "Bending analysis of embedded carbon nanotubes resting on an elastic foundation using strain gradient theory". In: *Acta Astronaut.* 119 (2016), pp. 1–12. DOI: 10.1016/j.actaastro.2015.10.021.

[42] Ç. Demir and Ö. Civalek. "On the analysis of microbeams". In: *Int. J. Eng. Sci.* 121 (2017), pp. 14–33. DOI: 10.1016/j.ijengsci.2017.08.016.

[43] Canadija M., Barretta R., de Sciarra F. M. "A gradient elasticity model of bernoulli-euler nanobeams in non-isothermal environments". In: *Eur. J. Mech. A Solids* 55 (2016), pp. 243–55.

[44] B. Babu, B. P. Patel. "Analytical solution for strain gradient elastic Kirchhoff rectangular plates under transverse static loading". In: *European Journal of Mechanics* A Solids.73 (2019), pp. 101–111.

[45] F. Cornacchia, F. Fabbrocino, N. Fantuzzi, R. Luciano, R. Penna. "Analytical solution of cross- and angle-ply nano plates with strain gradient theory for linear vibrations and buckling". In: *MECHANICS OF ADVANCED MATERIALS AND STRUCTURES* (). DOI: https://doi.org/10.1080/15376494.2019.1655613.

[46] F. Cornacchia, N. Fantuzzi, R. Luciano, R. Penna. "Solution for cross- and angle-ply laminated Kirchhoff nano plates in bending using strain gradient theory". In: *Composites Part B* 173.107006 (2019). DOI: https://doi.org/10.1016/j.compositesb.2019.107006.

[47] Barretta R., Feo L., Luciano R., Marotti de Sciarra F., Penna R. "Functionally graded timoshenko nanobeams: a novel nonlocal gradient formulation". In: *Compos. Part B: Eng.* 100 (2016), pp. 208–219.

[48] M. Bacciocchi, N. Fantuzzi, A. J. M. Ferreira. "Conforming and nonconforming laminated finite element Kirchhoff nanoplates in bending using strain gradient theory". In: *Composite Structures* 270.114084 (2021), pp. 101–111. DOI: https://doi.org/10.1016/j.compstruc.2020.106322.

[49] M. Bacciocchi, N. Fantuzzi, R.Luciano, A. M. Tarantino. "Linear eigenvalue analysis of laminated thin plates including the strain gradient effect by means of conforming and nonconforming rectangular finite elements'". In: *Computers and Structures* 257.106676 (2021). DOI: https://doi.org/10.1016/j.compstruc.2021.106676.

[50] N. Fantuzzi A. J. M. Ferreira. *MATLAB Codes for Finite Element Analysis*. Springer. ISBN: 978-3-030-47951-0.

[51] L. Leonetti, N. Fantuzzi, P. Trovalusci, F. Tornabene. "Scale Effects in Orthotropic Composite Assemblies as Micropolar Continua: A Comparison between Weak- and Strong-Form Finite Element Solutions". In: *Special Issue Behavior of Metallic and Composite Structures* (). DOI: ,https://doi.org/10.3390/ma12050758.

[52] Barretta R., Luciano R. "Analogies between Kirchhoff plates and functionally graded Saint-Senant beams under torsion". In: . *Continuum Mech. Thermodyn.* 27 (2015), pp. 499–505.

[53] Barretta R., Luciano R. "Exact solutions of isotropic viscoelastic functionally graded Kirchhoff plates". In: *Compos. Struct.* 118 (2014), pp. 448–454.

[54] S. Woinowsky-Krieger S. P. Timoshenko. *Theory of Plates and Shells*. McGraw-Hill, 1959.